Available online at www.sciencedirect.com
SCIENCE DIRECT®
Geochimica et Cosmochimica Acta 70 (2006) 408–425
Geochimica
www.elsevier.com/locate/gca

# Cretaceous black shales as active bioreactors: A biogeochemical model for the deep biosphere encountered during ODP Leg 207 (Demerara Rise)

Sandra Arndt [a,*], Hans-Jürgen Brumsack [a], Kai W. Wirtz [a,b]

[a] *Institute for Chemistry and Biology of the Marine Environment (ICBM), Oldenburg, Germany*
[b] *Institute for Coastal Research, GKSS Research Centre Geesthacht, Germany*

Received 21 December 2004; accepted in revised form 2 September 2005

**Abstract**

A transport–reaction model was designed to identify the combination and importance of biogeochemical processes operating in four sites drilled during ODP Leg 207 (Demerara Rise, Equatorial Atlantic). Almost 100 Ma after their deposition, deeply buried Cretaceous black shales still act as active bioreactors in great sediment depths and control the biogeochemical reaction network of the whole sediment column. According to a model calibrated at the four drill sites through inverse modeling techniques, methanogenesis could be identified as a key process that dominates not only organic matter degradation but also sulfate availability through the anaerobic oxidation of methane above the black shales. A complete depletion of sulfate within the black shale sequences promotes the remobilization of biogenic barium that reprecipitates as authigenic barite at the top of the sulfate depletion zone. Temporal dynamics of degradation processes caused continuous shifts of the barite precipitation zone during burial, thus inhibiting the formation of an authigenic barite front or causing the dissolution of earlier formed fronts. Major deviations of pore water sulfate profiles from a linear gradient coincide with depths of decelerated or accelerated transport caused by local porosity minima or maxima. Model-determined reaction rates are by far lower than those found in shallower sediments due to the low metabolic activities that are characteristic for the Deep Biosphere. But even after almost 100 Ma, changing organic matter quality still influences the degradation within the black shale sequences, as it is indicated by model results.
© 2005 Elsevier Inc. All rights reserved.

## 1. Introduction

First evidence of an active, microbial population in deep sediments was reported 20 years ago, when microbial activity was observed in sediment depths of about 150 m in the framework of the Deep Sea Drilling Program (DSDP) (Oremland and Polcin, 1982; Whelan et al., 1986; Tarafa et al., 1987). In recent years, the existence of prokaryotes down to sediment depths of 842 mbsf was proven (Parkes et al., 2000) and an extrapolation of cell counts at a small number of ODP Sites suggests that the biomass of the so-called Deep Biosphere constitutes one-tenth (Parkes et al., 2000) or even one-third (Whiteman et al., 1998) of the total global, living biomass. Today, increasing attention is paid to this intriguing but nearly nonaccessible environment (e.g., Parkes et al., 2000; D'Hondt et al., 2003, 2004). In particular, a more quantitative understanding of its biogeochemical key processes will be indispensable to evaluate its role in Earth's biogeochemical cycles. Nevertheless, our present understanding of the Deep Biosphere still remains extremely sparse, since it is characterized by a highly complex interplay of biological, chemical, and hydrostatic processes operating over a wide range of spatial and a characteristic range of temporal scales. The driving force behind the biogeochemical reaction network is the degradation of organic matter. While the availability of easily degradable organic matter is often limited to the shallow

* Corresponding author. Present address: Department of Earth Sciences—Geochemistry, Faculty of Geosciences, P. O. Box 80.021, 3508 TA, Utrecht University, Netherlands. Fax: +31 30 253 5302.
*E-mail address:* s.arndt@geo.uu.nl (S. Arndt).

0016-7037/$ - see front matter © 2005 Elsevier Inc. All rights reserved.
doi:10.1016/j.gca.2005.09.010

subsurface, deeply buried organic matter-rich black shales provide a suitable substrate for ongoing microbial activity in deep sediments (Krumholz et al., 1997; Coolen et al., 2002; Krumholz et al., 2002). These strata bear testimony of significant perturbations of the global ocean–atmosphere-system, the so-called oceanic anoxic events [OAE (e.g., Schlanger and Jenkyns, 1976; Arthur et al., 1990)]. OAEs are defined by massive, global deposition of organic carbon in marine environments, which occurred either as a consequence of increased water column preservation, increased oceanic productivity or both (Erbacher et al., 2001; Wilson and Norris, 2001; Brumsack, 2005).

Concentration–depth profiles of dissolved species are sensitive indicators of biogeochemical processes in the sediment. However, an intuitive identification of important processes on the basis of depth profiles is often not feasible, since the natural system dynamics are usually characterized by an extremely high degree of complexity. In this respect, mathematical modeling provide an ideal framework towards a better understanding of the mechanisms that control sediment biogeochemistry by formulating and testing hypothetical mechanisms. As it allows a quantitative assessment of biogeochemical processes, it can be, in careful combination with observations, of extraordinary explanatory power and might, therefore, provide a key to one of the last unknown environments on Earth.

Sediment sequences drilled at Demerara Rise (Equatorial Atlantic) during ODP Leg 207 are characterized by deeply buried sequences of Cretaceous black shales (Shipboard Scientific Party, 2004). With a total number of 152 samples and a relatively high spatial resolution, the interstitial water sampling program conducted during ODP Leg 207 is unique among the few other interstitial water data sets taken at black shale bearing ODP sites, like ODP Leg 122, Exmouth Plateau (Shipboard Scientific Party, 1990) and ODP Leg 159, Côte d'Ivoire (Shipboard Scientific Party, 1996). Especially with respect to the extended ODP data set, the detailed interstitial water data provide an ideal setting for a modeling study of the biogeochemical reaction network in deep, black shale bearing sediments. By designing a transport–reaction model we intended to identify the coupling and importance of various processes operating in four sites (sites 1257–1260) drilled during ODP Leg 207. Uncertainties in model parameters were constrained for each site using inverse modeling techniques. Our study is one of the first quantitative descriptions of biogeochemical processes in the Deep Biosphere. We aim to resolve the biogeochemical reaction network at Demerara Rise and to propose a first estimate of the most pertinent kinetic rate constants, thereby creating a basis for future studies.

## 2. Materials and methods

### 2.1. Site description

Demerara Rise is a prominent submarine plateau located at ca. 5°N off the coasts of Surinam and French Guyana (Fig. 1). It is built on rifted continental crust of Precambrian and early Mesozoic age and was one of the last areas in contact with West-Africa prior to the opening of the equatorial Atlantic. The rise stretches ca. 380 km along the coast and reaches a width of ca. 220 km from the shelf

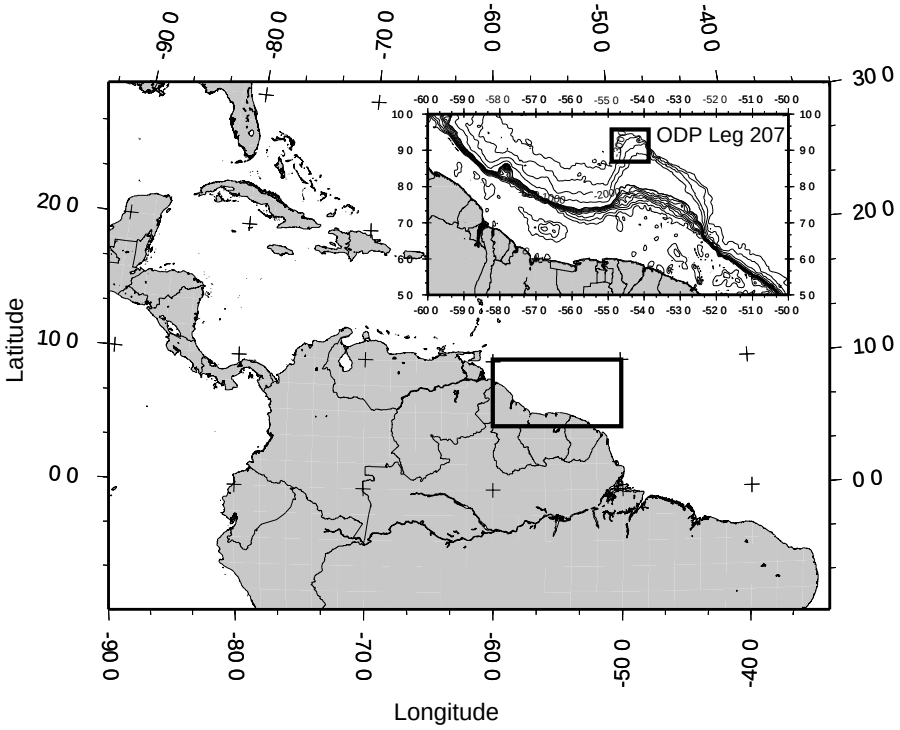


Fig. 1. Location of ODP Leg 207, Demerara Rise (Equatorial Atlantic).

break to the northeastern escarpment, where water depths increase sharply from 1000 to over 4500 m. While most of the plateau lies in shallow water (700 m), the northwest margin is a gentle ramp that reaches depths of 3000–4000 m. Here the plateau is covered by 2–3 km of pelagic sediment down to water depths >4000 m.

Sediment sequences drilled at Demerara Rise are of lower Albian to Neogene origin, thus reflecting a significant part of the paleoceanographic history of the tropical Atlantic Ocean. Upper Albian sediments are mostly green clayey carbonate siltstones. The Cenomanian to Santonian sequence consists almost exclusively of laminated black shales with occasional stringers of limestone and chert. In total, ca. 650 m of black shales were recovered during ODP Leg 207 (Shipboard Scientific Party, 2004). Critical intervals recovered include multiple copies of OAEs 2 and 3. Campanian to Paleogene sediments are calcareous to siliceous oozes and chalks. A prominent submarine channel system and erosional surface developed in the late Oligocene to early Miocene. The channels carried sediment east-to-west over the flank of the plateau and into feeder channels for a submarine fan that formed northwest of the Demerara Rise. The channel system was short-lived and most of the Neogene sediments (hemipelagic and pelagic deposits) are thin or absent from the distal portions of the plateau.

### 2.2. Sampling methods

During ODP Leg 207 interstitial waters from 152 samples, covering a depth range from the sediment/seawater interface to 548 mcd (meters composite depth), were collected and processed using standard ODP methods (Gieskes et al., 1991). Interstitial water samples were usually squeezed from whole-round samples immediately after retrieval of the cores using titanium squeezers, modified after the standard ODP stainless steel squeezer (Manheim and Sayles, 1974). At "critical boundaries," e.g., close to the C/T-interval, half-round sections were taken to minimize core loss and were then treated in the same way as whole-round samples. Interstitial water samples were analyzed onboard. Salinity was routinely determined as total dissolved solids with a Goldberg optical handheld refractometer. The pH and alkalinity were analyzed by Gran titration with a Brinkmann pH electrode and a Metrohm autotitrator. Dissolved chloride was determined by titration with silver nitrate. Ammonium was measured by spectrophotometric methods (Gieskes et al., 1991) using a Milton Roy Spectronic 301 spectrophotometer equipped with a sample introduction system. Barium concentrations were determined by inductively coupled plasma-atomic emission spectroscopy (ICP-AES) following the general procedure outlined by Murray et al. (2000). Sulfate was analyzed at the Institute for Chemistry and Biology of the Marine Environment (ICBM) in Oldenburg using liquid XRF. The analytical procedure applied to sulfate measurements mainly followed the procedure described by Wehausen et al. (1999). A 5 ml volume of the sample solution was pipetted into polyethylene cups supported by a 6.3 μm polypropylene thin film (Somar, Tuckahoe, USA). Calibration was based on a dilution series of a standard solution. Sulfate was measured at its most sensitive line (Kα). An additional adjustment of the calibration curve, based on repeated measurements of two sulfate dilution series, as well as an increase of sulfur measurement time from 10 to 20 s, provide a higher accuracy in the critical range of low sulfate concentrations. The reproducibility of results was ensured via multiple determinations of the International Association for the Physical Sciences of the Ocean (IAPSO) standard seawater (alkalinity, $Cl^-$ and $SO_4^{2-}$), spiked synthetic seawater (ICP-AES determinations), or through the use of a calibration curve ($NH_4^+$). Methane was determined by headspace measurements following the standard procedure described by Kvenvolden and McDonald (1986). Immediately after core retrieval on deck, a 5 $cm^3$ sediment sample was collected using a borer tool, placed in a 21.5 $cm^3$ glass serum vial, and sealed on deck or immediately in the laboratory with a septum and metal crimp cap. For consolidated or lithified samples, chips of material were placed in the vial and sealed. Prior to gas analysis, the vial was heated at 70 °C for 30 min. A 5 $cm^3$ subsample of the headspace gas was extracted from each vial using a glass gas syringe. Methane contents of gas samples were analyzed using the shipboard GC3 gas analysis system and the natural gas analyzer when elevated gas contents were observed. Although samples for gas analysis are collected almost immediately after the sediment cores reach the ship, most of the interstitial methane outgases during core recovery and methane measurements, thus, reflect the gas-saturation concentration at surface conditions. Measured methane concentrations are, therefore, generally underestimated and scattered.

## 3. Model description

A numerical model was designed to identify the combination and importance of various processes operating in sediments at Demerara Rise. One-dimensional conservation of dissolved species $C_i$ in sediment is referred to as the General Diagenetic Equation (Berner, 1980) and is given by

$$\frac{\partial \phi C_i}{\partial t} = -\frac{\partial F_i}{\partial z} + \phi \sum R_i, \quad (1)$$

where $\phi$ denotes the porosity. Temporal change in pore water concentration of chemical species $i$ is balanced by the divergence of mass flux $F_i$ with $F_i = D_i \partial C_i / \partial z$ (see Eq. (A.1) in Appendix A) and the sum of reactions $\sum R_i$. A more detailed description of the model is given in Appendix A.

### 3.1. Implementation

Steady state profiles of dissolved species were calculated applying finite difference techniques. Based on the operator

splitting approach, transport and reaction equations were solved separately. At the beginning of each time-step, the reaction equations were integrated using the Euler–Forward method. To ensure numerical stability, the time-step was automatically adjusted, where necessary, so that the change in concentration per time-step equals 10% of total concentration at the most. The transport equations were solved applying the semi-implicit Crank–Nicolson scheme solved iteratively by successive over-relaxation with Chebyshev acceleration and odd–even ordering. The algorithm was run with a maximum time-step of $\Delta t = 100$ a and an equally spaced spatial resolution of $\Delta z = 1$ m until steady state as defined by $|C_{i,t} - C_{i,t-1}| < 1 \times 10^{-4} \cdot C_{i,t}$ was reached. Computational time was shortened by setting the initial conditions for solute concentrations near the observed profiles. Initial conditions for solid species are chosen on the basis of measurements (Hetzel, 2003; Shipboard Scientific Party, 2004). The organic carbon content in sediments from Demerara Rise reveals a marked contrast between the black shale sequences, which are characterized by high values in a range between 1 and 30 wt.%, and the rest of the sediment column, which generally shows low contents of <0.1 wt.% with slightly elevated values in Albian siltstones below the black shales (Fig. 6). Since interstitial sulfate profiles indicate that sulfate reduction is negligible in the upper sediment column, the organic carbon content was set to zero at these depths. Due to their lamination and occasional stringers of limestone and chert, the black shale sequences show a scatter of organic carbon contents. Therefore, an average value was generally used throughout the black shale sequences. At site 1259, the black shale sequence was, however, divided in two parts, since very high organic carbon contents in combination with high methane concentrations were observed at their lower boundary (Fig. 6). Albian siltstones are characterized by slightly elevated organic carbon contents. Yet, Rock-Eval pyrolysis of these samples identifies the organic matter as a mixture of types II and III, which is less suitable for degradation (Meyers et al., 2004; Shipboard Scientific Party, 2004) and organic carbon contents were, therefore, set to zero. Compared to the other three sites, Albian mudstones at site 1258 reveal, however, much higher average organic carbon contents (4.2 wt.%) and a higher organic carbon content is, thus, assumed for these depths (Fig. 6). Solid species are not transported in the model. This assumption is valid in the time range, which is needed by the model to reach steady state pore water profiles, since present sedimentation rates at Demerara Rise are extremely low ($6.7-15 \times 10^{-6}$ m a$^{-1}$) and compaction at these depths is negligible (Shipboard Scientific Party, 2004).

Measured pore water concentrations are provided as boundary conditions at the sediment water interface. The choice of appropriate lower boundary conditions is, however, a difficult task, as drilling operations were usually stopped in the top few meters of Albian sediments. Consequently, simulated processes in the black shales might be driven to a certain extent by the lower boundary conditions. In particular, the lower boundary condition for methane is difficult to constrain.

Nevertheless, the detailed ODP data set provides a set of additional information and boundary conditions can be constrained not only on the basis of pore water measurements but also according to lithostratigraphic observations, gas compositions or TOC measurements (Shipboard Scientific Party, 2004). Head space measurements, for instance, indicate a moderate or even an abrupt decrease of methane concentrations below the black shales (Meyers et al., 2004) and organic matter of Albian sediments is, because of its type, less suitable for degradation (Shipboard Scientific Party, 2004). Thus, we consider a Dirichlet or fixed concentration boundary condition more appropriate to describe processes at the lower boundary. The constant and site-specific parameter values used in the model are summarized in Tables 1 and 2, respectively.

Porosity profiles at Demerara Rise exhibit usually declining porosity values intercepted by low- and high-porosity horizons (Shipboard Scientific Party, 2004). The notable association between these horizons and discontinuities in depth profiles of dissolved species indicates that these porosity changes exert a strong physical control on the transport of dissolved species. Thus, a number $n$ of low- and high-porosity layers of Gaussian form were super-

Table 1
Fixed parameter values and boundary conditions used in the model

| Symbol | Description | Value | Unit |
|---|---|---|---|
| $D_{SO_4}$ | Molecular diffusion coefficient for $SO_4^{2-}$ | 0.017 | m$^2$a$^{-1}$ |
| $D_{CH_4}$ | Molecular diffusion coefficient for $CH_4$ | 0.028 | m$^2$a$^{-1}$ |
| $D_{Ba}$ | Molecular diffusion coefficient for $Ba^{2+}$ | 0.012 | m$^2$a$^{-1}$ |
| $D_{NH_4}$ | Molecular diffusion coefficient for $NH_4^{2-}$ | 0.035 | m$^2$a$^{-1}$ |
| $C_{SO_4,BW}$ | Bottom water $SO_4^{2-}$ concentration | 28 | mM |
| $C_{CH_4,BW}$ | Bottom water $CH_4$ concentration | 0 | mM |
| $C_{Ba,BW}$ | Bottom water $Ba^{2+}$ concentration | 0 | mM |
| $C_{NH_4,BW}$ | Bottom water $NH_4$ concentration | 0 | mM |
| $C_{SO_4,z_{max}}$ | $SO_4^{2-}$ concentration at the bottom of the sediment column | 0 | mM |
| C/N | Carbon–nitrogen ratio of organic matter | 20 | |
| $K_{NH_4}$ | Adsorption constant for ammonium adsorption | 1.3 | |
| $K_S$ | Half-saturation constant for sulfate reduction (organic matter degradation) | 1.6 | mM |
| $K_{S,AMO}$ | Half-saturation constant for sulfate reduction (AMO) | 1 | mM |

Table 2
Values of site-specific parameters and boundary conditions used in the model

| Symbol | Description | Unit | Site 1257 | Site 1258 | Site 1259 | Site 1260 |
|---|---|---|---|---|---|---|
| $C_{CH_4,z_{max}}$ | $CH_4$ concentration at the bottom of the sediment column | mM | 0.8 | 1 | 1 | 0.8 |
| $C_{Ba,z_{max}}$ | $Ba^{2+}$ concentration at the bottom of the sediment column | μM | 0.0 | 20 | 300 | 0.0 |
| $C_{NH_4,z_{max}}$ | $NH_4$ concentration at the bottom of the sediment column | mM | 0.6 | 1.4 | 1.5 | 2.3 |
| $C_{CH_2O}(0)$ | POC concentration in black shales | wt.% | 6.55 | 7.79 | 7.92 for $z = [495, 538$ mcd$]$<br>16.36 for $z = [539, 549$ mcd$]$ | 7.44 |
| $C_{BaSO_4}(0)$ | Initial barite concentration in black shales | ppm | 500 | 500 | 1000 | 500 |

imposed on a linear or exponential porosity–depth relationship

$$\phi(z) = f(z) + \sum_i c_i \cdot e^{\left(-\frac{(z-d_i)^2}{f_i}\right)}, \quad (2)$$

where $f(z)$ is a linear function at sites 1257, 1258, and 1260, and an exponential one at site 1259. The fitted porosity–depth relationships used in the model are listed in Table 3. The measured as well as the fitted porosity profiles are shown in Fig. 2.

Table 3
Porosity $\phi$ versus depth $z$ (mcd) relationships for all model sites

Site 1257
$$\phi(z) = 0.67 - 1.32 \times 10^{-3} z - 0.12 \cdot e^{-\left(\frac{z-70}{25}\right)^2} + 0.2 \cdot e^{-\left(\frac{z-72}{6}\right)^2} + 0.11 \cdot e^{-\left(\frac{z-147}{10}\right)^2} + 0.25 \cdot e^{-\left(\frac{z-205}{25}\right)^2}$$

Site 1258
$$\phi(z) = 0.24 + 0.41 \cdot e^{(-2\times10^{-3} z)} + 0.12 \cdot e^{-\left(\frac{z-33}{10}\right)^2} - 0.03 \cdot e^{-\left(\frac{z-172}{40}\right)^2}$$

Site 1259
$$\phi(z) = 0.8 - 8.8 \times 10^{-4} z - 0.23 \cdot e^{-\left(\frac{z+25}{70}\right)^2} - 0.22 \cdot e^{-\left(\frac{z-95.5}{8}\right)^2} - 0.1 \cdot e^{-\left(\frac{z-130}{6}\right)^2} - 0.1 \cdot e^{-\left(\frac{z-466}{20}\right)^2} + 0.1 \cdot e^{-\left(\frac{z-520}{27}\right)^2}$$

Site 1260
$$\phi(z) = 0.74 - 1 \times 10^{-3} z - 0.25 \cdot e^{-\left(\frac{z-11}{20}\right)^2} + 0.27 \cdot e^{-\left(\frac{z-442}{50}\right)^2}$$

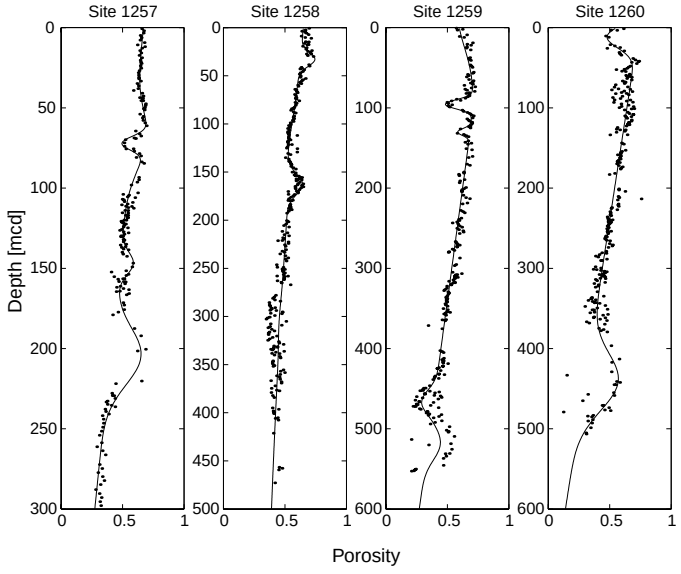


Fig. 2. Fitted (line) and measured (dots) porosity–depth profiles at Demerara Rise (sites 1257–1260). Fitted porosity–depth functions are listed in Table 3.

According to Eqs. (A.10) and (A.11), the stoichiometric solubility product of barite is influenced by salinity, temperature, and pressure. The temperature–depth relationship is controlled by the geothermal temperature gradient. The local pressure is calculated by summing the hydrostatic pressure of the overlaying water column as well as the static pressure of the sediment column, taking into account its density (Shipboard Scientific Party, 2004).

One of the prominent features in interstitial waters from ODP Leg 207 is the presence of brines at sites 1257 and 1259 characterized by chloride concentrations >60% higher than standard seawater (Shipboard Scientific Party, 2004). Maximum chloride concentrations are centered in the black shale sequences, decreasing above and below this unit, thus suggesting that the brines are sourced externally through the black shales. Unlike sites 1257 and 1259, site 1258 and 1260 pore waters are not characterized by the presence of brines (Shipboard Scientific Party, 2004). Salinity and chlorinity decrease with depth, reaching minimum values at the base of the drill holes. Measured salinity values were interpolated by using the piecewise cubic Hermite interpolation method (Fig. 3).

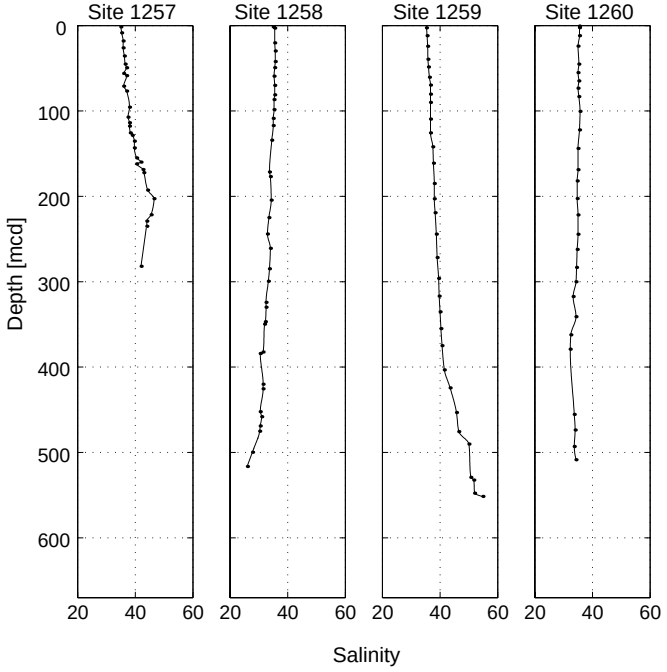


Fig. 3. Salinity depth profiles at Demerara Rise (sites 1257–1260). Measured salinities (dots) were interpolated cubically (line).

### 3.2. Inverse modeling

The Deep Biosphere is still one of the last mysterious environments on Earth. Exceptional environmental conditions impede a direct estimation of parameters on the basis of other modeling studies, generally dealing with processes in shallow sediment depths. Moreover, model parameters often represent the integrative influence of different processes which are not explicitly considered in model formulations and are, thus, hard to be confined. In such cases, inverse modeling techniques provide a comprehensive route to settle unknown model parameters based on available empirical data. Assuming that the rank of a parameter set depends on the similarity between simulated and measured data, an optimal parameter set that leads to the best fit of modeled interstitial water profiles can be determined. This is done by minimizing a cost function, typically a measure of the misfit between model results and observations. The cost functions $M_i(\vec{p})$ of each species $i$ depending on a variable parameter set $\vec{p}$ are formulated as the sum of the least-squares differences between simulated $C_{i,z}^{\mathrm{sim}}(\vec{p})$ and measured concentrations $C_{i,z}^{\mathrm{obs}}$ at each depth $z$, weighted by their respective measurement error $\sigma_i^2$. To avoid an overweighting of depths characterized by a high sample density, model results and observations were averaged over appropriate depth intervals $z$ (indicated by a bar). The cost function $M_{\mathrm{tot}}$, which has to be minimized, is then simply the sum over the determined cost functions of each species $i$:

$$M_i(\vec{p}) = \frac{1}{z}\sum_z \left(\frac{\bar{C}_{i,z}^{\mathrm{obs}} - \bar{C}_{i,z}^{\mathrm{sim}}(\vec{p})}{\sigma_i}\right)^2, \tag{3}$$

$$M_{\mathrm{tot}} = \frac{1}{i}\sum_i M_i(\vec{p}). \tag{4}$$

The choice of the minimization algorithm is a critical step in inverse modeling, since the shape of the cost function in the parameter space may reveal, in addition to a global minimum, multiple local minima, in which the algorithm can easily become trapped. However, the low cost of forward modeling, the low number of unknown parameters (<10), as well as the weak nonlinearity of the problem allowed the application of an extremely simple but reliable method, a Monte Carlo direct search technique with a uniform random sampler. The parameter space was sampled by drawing 1000 random parameter vectors out of a reasonably constrained parameter range. Hereafter, sampling was concentrated in the region of local minimum values by drawing 300 parameter vectors out of a parameter range, which was adapted to the magnitude of the parameter's gradient in the parameter space. Thereby, a set of model parameters has been determined for each site (Table 4). The parameter values are not completely independent of each other. A stepwise, simultaneous variation of parameter couples reveals a correlation between fitted parameter values or a nonlinear fitness landscape, respectively. A low rate constant of anaerobic methane oxidation, for instance, would lead to a penetration of sulfate into the black shale layer as a consequence of the decreased consumption above the black shales. Consequently, high values of the cost function are found for low AMO rate constants (Fig. 4). Increasing values of the rate constant of sulfate reduction can, however, compensate this trend to a certain degree. Higher sulfate reduction rates induce a fast consumption of sulfate in the top few centimeters of the black shales and, thus, lower values of the cost function. However, the value of the cost function becomes virtually independent of the sulfate reduction rate constant if the AMO rate constant reaches a value which is sufficiently high to consume the pore water sulfate above the black shales. In the area of increasing AMO rate constants, the cost function shows another, even though, lower increase, since the sulfate penetration depth is shifted upwards by an enhanced consumption.

Table 4
Rate constants for methanogenesis $k_{\mathrm{G,CH_4}}$, sulfate reduction $k_{\mathrm{G,SO_4}}$, anaerobic oxidation of methane $k_{\mathrm{AMO}}$, barite dissolution $k_{\mathrm{diss,BaSO_4}}$, and barite precipitation $k_{\mathrm{prec,BaSO_4}}$

| Site | $k_{\mathrm{G,CH_4}}$ ($\mathrm{a}^{-1}$) | $k_{\mathrm{G,SO_4}}$ ($\mathrm{a}^{-1}$) | $k_{\mathrm{AMO}}$ ($\mathrm{a}^{-1}$) | $k_{\mathrm{diss,BaSO_4}}$ ($\mathrm{a}^{-1}$) | $k_{\mathrm{prec,BaSO_4}}$ ($\mu\mathrm{M\ a}^{-1}$) |
|---|---|---|---|---|---|
| 1257 | $1.5\times10^{-9}$ | $1\times10^{-8}$ | $4\times10^{-4}$ | $3\times10^{-8}$ | $5\times10^{-4}$ |
| 1258 | $2.5\times10^{-9}$ | $1\times10^{-8}$ | $2\times10^{-4}$ | $3\times10^{-8}$ | $5\times10^{-4}$ |
| 1259 | $3.5\times10^{-9}$ | $1\times10^{-8}$ | $3\times10^{-4}$ | $3\times10^{-8}$ | $5\times10^{-4}$ |
| 1260 | $3.1\times10^{-9}$ | $1\times10^{-8}$ | $4\times10^{-4}$ | $3\times10^{-8}$ | $5\times10^{-4}$ |

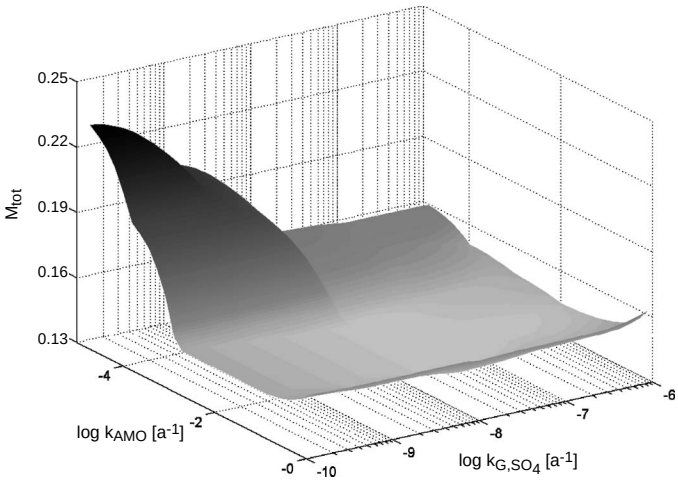


Fig. 4. Distribution of the cost function $M_{\mathrm{tot}}$ over a two-dimensional parameter space (site 1257). The rate of constant of anaerobic methane oxidation $k_{\mathrm{AMO}}$ and sulfate reduction $k_{\mathrm{G,SO_4}}$ are varied simultaneously. All other parameters are held constant at the values indicated in Table 4.

## 4. Results and discussion

### 4.1. Biogeochemical processes at Demerara Rise

Concentration–depth profiles of dissolved and solid species reveal nearly identical patterns (Fig. 5) (Shipboard

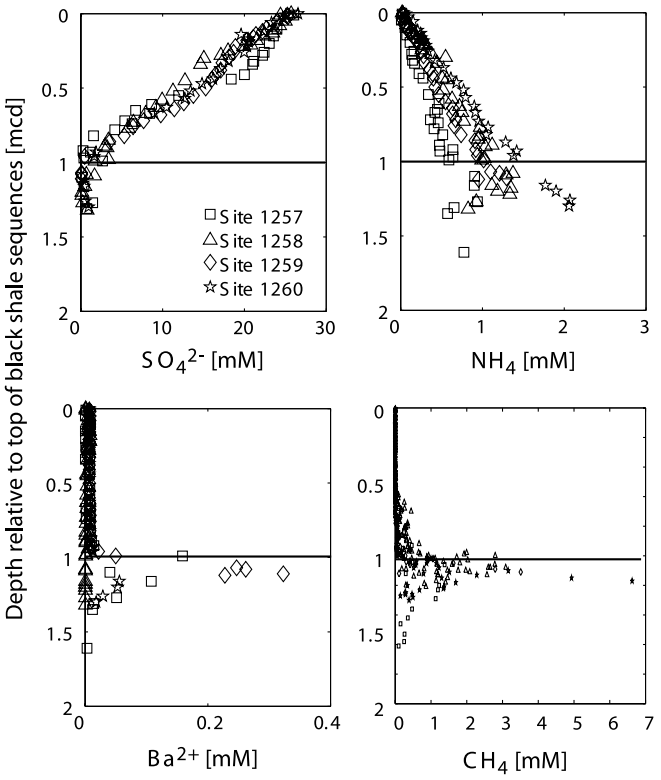


Fig. 5. Measured interstitial water profiles of sulfate, ammonium, barium, and methane at four drilling sites (sites 1257–1260, Demerara Rise). The depth is given relative to the top of the respective black shale sequence.

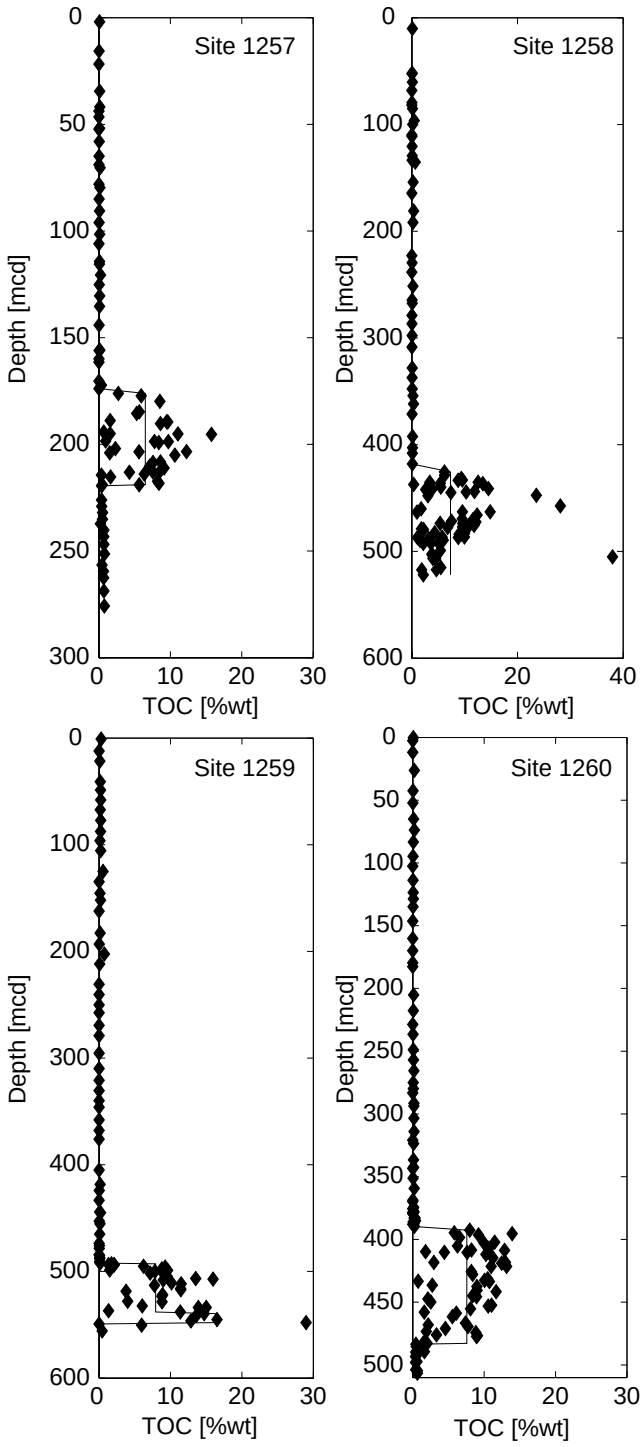


Fig. 6. Measured organic carbon contents (diamonds) and assumed organic carbon contents in the model (line) at four drilling sites (sites 1257–1260, Demerara Rise).

Scientific Party, 2004). The most striking feature of the organic carbon profiles is the presence of the deep-seated, laminated black shale sequences, which exhibit very high values up to 30 wt.% (Fig. 6). While the underlying calcareous claystones at site 1258 show smaller, though still elevated, organic carbon contents, underlying sediments at the other sites, as well as overlying Campanian to Pleistocene chalks and oozes reveal relatively low organic carbon concentrations. Pore water chemistry is to a large extent controlled by the organic matter-rich Cretaceous black shale sequences. Pore water sulfate concentrations decrease almost linearly from typical seawater values near the sediment/water interface to values close to zero a few meters above the top of the black shale unit. On the contrary, pore water ammonium reveals maximum concentrations between 0.8 and 2 mM in the black shales and slightly lower values in underlying Albian sediments. Above the black shale sequences ammonium decreases quasi-linearly towards the sediment/water interface, where ammonium concentrations close to detection limit indicates its oxidation in the very shallow subsurface. Linearity of sulfate and ammonium profiles indicates the minor importance of sulfate reduction at shallower depth intervals. Major deviations of the depth profiles from a linear gradient coincide with local porosity maxima or minima. Due to the depth-dependent porosity, two pseudo-advective terms arise in the transport equation (Eq. (A.1)), leading to kinked profiles as a consequence of an accelerated or decelerated transport. Downhole profiles are controlled by the existence of one major stratigraphic source/sink and simple compensatory downward diffusion to/from the sediment/water interface in the absence of the accumulation of significant sediments younger than middle Eocene age.

High methane/ethane ratios, as well as the absence of heavier hydrocarbons, indicate a biogenic production of methane in the black shales (Shipboard Scientific Party, 2004). The methane production is rather dominated by the reduction of interstitial $CO_2$ than by in situ microbial fermentation of marine organic matter (Meyers et al., 2004). Methane production is accompanied by the increase in ammonium, a common by-product of organic matter consumption. The upward diffusion of methane may support metabolic activity such as AMO at the bottom of the sulfate penetration zone where methane concentrations rapidly decrease to background concentrations. The complete depletion of sulfate above the black shale sequences promotes the remobilization of biogenic barium in organic matter-rich sediments (Brumsack and Gieskes, 1983; Torres et al., 1996; Bréhéret and Brumsack, 2000). Barium profiles are mainly governed by barite solubility (Church and Wohlgemuth, 1972) and reveal pronounced maxima reaching values between 50 and 300 μM in the black shales (Fig. 5). Concentrations decrease at the top of the sulfate depletion zone in overlaying Upper Cretaceous chalks, where authigenic barite crystals of millimeter to centimeter scale are frequently observed (Shipboard Scientific Party, 2004). Although, barium profiles may be prone to slight contamination by seawater due to the use of ODP's rotary core barrel (RCB) drilling technology, the shape of barium profiles together with the extensive sedimentological evidence indicates intense barium mobilization in the black shales.

Interstitial water profiles from Demerara Rise are very similar to those from the Exmouth Plateau (Shipboard Scientific Party, 1990) and the Ghana Transform Margin (Shipboard Scientific Party, 1996). They all exhibit a linear decrease of sulfate towards its complete depletion at the top of the black shale sequences. Maximum ammonium and methane concentrations coincide with elevated organic matter contents and they compare well with concentrations found at Demerara Rise. Methane concentrations rapidly decrease above the black shales.

### 4.2. Sensitivity of biogeochemical key processes

As the dynamics of a sedimentary system generally reveal a high degree of complexity, an intuitive identification of essential processes is often unfeasible. With a systematic variation of system parameters, initial and boundary conditions the relative importance of modeled processes is assessed. The sensitivity of the model response is expressed as the depth averaged, percentage deviation $d_i$ between the simulated pore water concentrations after the variation of one parameter value $C(\vec{p})_i$ and the modeled concentrations of a standard parameter set $C(\vec{p}_{\mathrm{std}})_i$ (see Table 4, Site 1260) for each species $i$ at site 1260.

Model parameters can be divided in two groups. The first set of parameters plays a crucial role for the evolution of certain concentration depth profiles, but does not affect the spatial evolution of other species like the rate constants for barite dissolution and barite precipitation, for instance.

Essentially, the shape of concentration–depth profiles at Demerara Rise is influenced by two major biogeochemical processes: the decomposition of organic matter in the black shales and AMO above the black shale sequences. A change in one of these rate constants affects not only directly involved species, but influences also concentration depth profiles of other species, mainly through the availability of sulfate. Nevertheless, the quantitative changes of concentration–depth profiles as a consequence of an increase or decrease of respective rate constants differ considerably. A modification of sulfate reduction rate, for instance, becomes important when significant amounts of sulfate are available for the degradation of organic matter in the black shales. In the case of its complete depletion above the black shales, the influence of a decrease or increase in the rate constant of sulfate reduction only leads to deviations of −4 and 0.5% for sulfate profiles and even smaller values for other species and is, therefore, negligible. AMO is one of the biogeochemical key processes in sediments from Demerara Rise, since it represents the link between sedimentary C and S cycles. Consequently, a change of its rate constant affects sulfate and methane, and to a lesser extent also the barium depth profile. Methanogenesis is by far the most dominant process in sediments from Demerara Rise. It controls the shapes of methane, ammonium, and sulfate depth profiles to a significant extent and influences barite dynamics through the availability of sulfate. Generally, a change in methanogenic rate constant has a greater overall influence on all concentration–depth profiles than any other parameter value. The ammonium profile, for instance, reveals a deviation of 20% as a consequence of an increased methanogenic rate constant, whereas an increase in its lower boundary condition only results in a 10% relative deviation. A modification of the lower boundary condition for methane enhances or reduces the upward diffusional flux of methane and has, thus, a direct influence on the estimates of reaction rate constants. In particular, the rate constant of methanogenesis depends on the choice of the lower boundary condition for methane. Fig. 7 illustrates the effect of different, lower boundary conditions for methane. Higher boundary concentrations or a no-flux condition cause an enhanced upward diffusion of methane and would, consequently, lead to lower estimates of methanogenic rate constants. The impact of a change in the lower boundary condition for methane on model-determined rate constants only becomes significant when very high boundary concentrations or a no-flux boundary condition are applied. However, methane measurements do not indicate concentrations in this range nor do they support a no-flux boundary condition (Meyers et al., 2004). In addition, a change in boundary condition has no effect on the order of magnitude of methanogenic rate constants since even small changes in methanogenic rates reveal a significant effect on sulfate penetration depths.

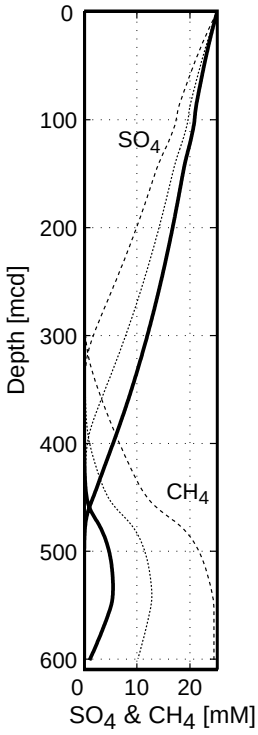


Fig. 7. Sulfate and methane depth profiles simulated with constant lower boundary condition for methane of $CH_{4,zmax} = 1$ mM (solid line), $CH_{4,zmax} = 10$ mM (dotted line), and a no-flux condition (dashed line).

### 4.3. Cretaceous black shales as diagenetic bioreactors

Almost 100 Ma after their deposition, Cretaceous black shales at Demerara Rise still provide a suitable substrate for ongoing microbial activity in deep sediments. Model results (Fig. 8) indicate that degradation of organic matter is dominated by methanogenesis with first-order decay constants between $1 \times 10^{-9}$ and $3.5 \times 10^{-9}$ $a^{-1}$. Elevated (sites 1257 and 1259) as well as reduced salinities (sites 1258 and 1260) do not seem to stimulate or inhibit the metabolic activity of methanogenic bacteria, since methanogenic rate constants do not vary significantly between high and low salinity sites. The stimulation of bacterial activity by brine intrusion is often a consequence of the enhanced supply of sulfate, which may be enriched in brine fluids (e.g., Cragg et al., 1992; D'Hondt et al., 2004). Brines at Demerara Rise are, however, sulfate-depleted, as it is indicated by element/chloride depth profiles. An inhibition of dissimilatory metabolism is thought to be related to bioenergetic constraints. Since methanogenic archaea use organic solutes to create an osmotic balance, culture studies indicate that the cost of adaptation exceeds the energy gain at a salt concentration of 120 g/L NaCl (Oren, 2002). Nevertheless, metabolically active microbial communities are known from a number of deep, high salinity environments (e.g., Dickins and van Vleet, 1992; Kotelnikova, 1992; Eder et al., 2001). Recently, microbial activity was discovered in one of the most extreme saline environments on earth, the Discovery basin (van der Wielen et al., 2005).

The simulated rate constants are far lower than those determined for subsurface environments (e.g., Canfield, 1994; Tromp et al., 1995), reflecting not only the extremely slow metabolic activity in the Deep Biosphere, but also the low quality of type II/III organic matter exhibiting C/N ratios between 16.2 and 44.7 (Shipboard Scientific Party, 2004). In marine sediments, degradation rate constants can vary over a range of eight orders of magnitude (Canfield, 1994) and typically show a continuous decrease with time due to preferential consumption of easily degradable fractions during early diagenesis. Middelburg (1989) determined an empirical $k$–$t$ relationship on the basis of laboratory and field measurements, validated in a time range of 0–6 Ma. In his so-called power model, the first-order rate parameter, $k$, decreases with time $t$ according to the power function,

$$k(t) = 0.16 \cdot (a + t)^{-0.95}. \quad (5)$$

The apparent initial age $a$ accounts for differences in reactivity at the sediment/water interface and varies in a range between 0.09 a (fresh plankton) and 35,000 a (central Pacific) (Middelburg, 1989). For organic matter of Cretaceous origin (ca. 95 Ma) one would calculate a first-order rate constant in an order of magnitude of $10^{-9}$ $a^{-1}$. This first estimate is in good agreement with the rate constant for methanogenesis determined by inverse modeling techniques. Furthermore, model-determined methanogenic rates (Table 5) agree well with maximum rates of $H_2/CO_2$ methanogenesis in deep sediments (below 100 m) from the Japan Sea (ODP Leg 128), the Cascadia Margin (ODP Leg 146), and the Blake Ridge (ODP Leg 164), ranging from 0.63 to 3.65 μM $a^{-1}$ (Parkes et al., 2000). The similarity of these methanogenic rates indicates that factors, such as bacterial biomass, metabolic requirements or organic matter quality, are responsible for limiting conditions in deep sediments rather than organic carbon concentrations.

Nevertheless, the high amounts of organic carbon in the black shale sequences are providing a source of carbon and energy for ongoing microbial activity since almost 100 Ma. Yet, little can be said about the temporal dynamics of degradation processes. Especially the temporal evolution of organic matter concentrations in the black shales, their initial organic carbon contents, and their degradation rate constants could provide a better understanding of diagenetic processes below the shallow subsurface environment and Cretaceous environmental conditions at Demerara Rise. In this respect, the power model is a useful tool that can be applied to backtrack temporal processes and to give an idea of the initial organic matter content $G(0)$ in the Cretaceous sediments. By substituting Eq. (5) into first-order kinetics of organic matter decomposition one obtains, after integration,

$$G(t) = G(0) \cdot e^{3.2 \cdot (a^{1/20} - (a+t)^{1/20})}. \quad (6)$$

An intuitive estimation of the apparent initial age of Cretaceous organic matter is hardly feasible, since oceanic anoxic events are characterized by extreme environmental conditions that are still a matter of debate. Nevertheless,

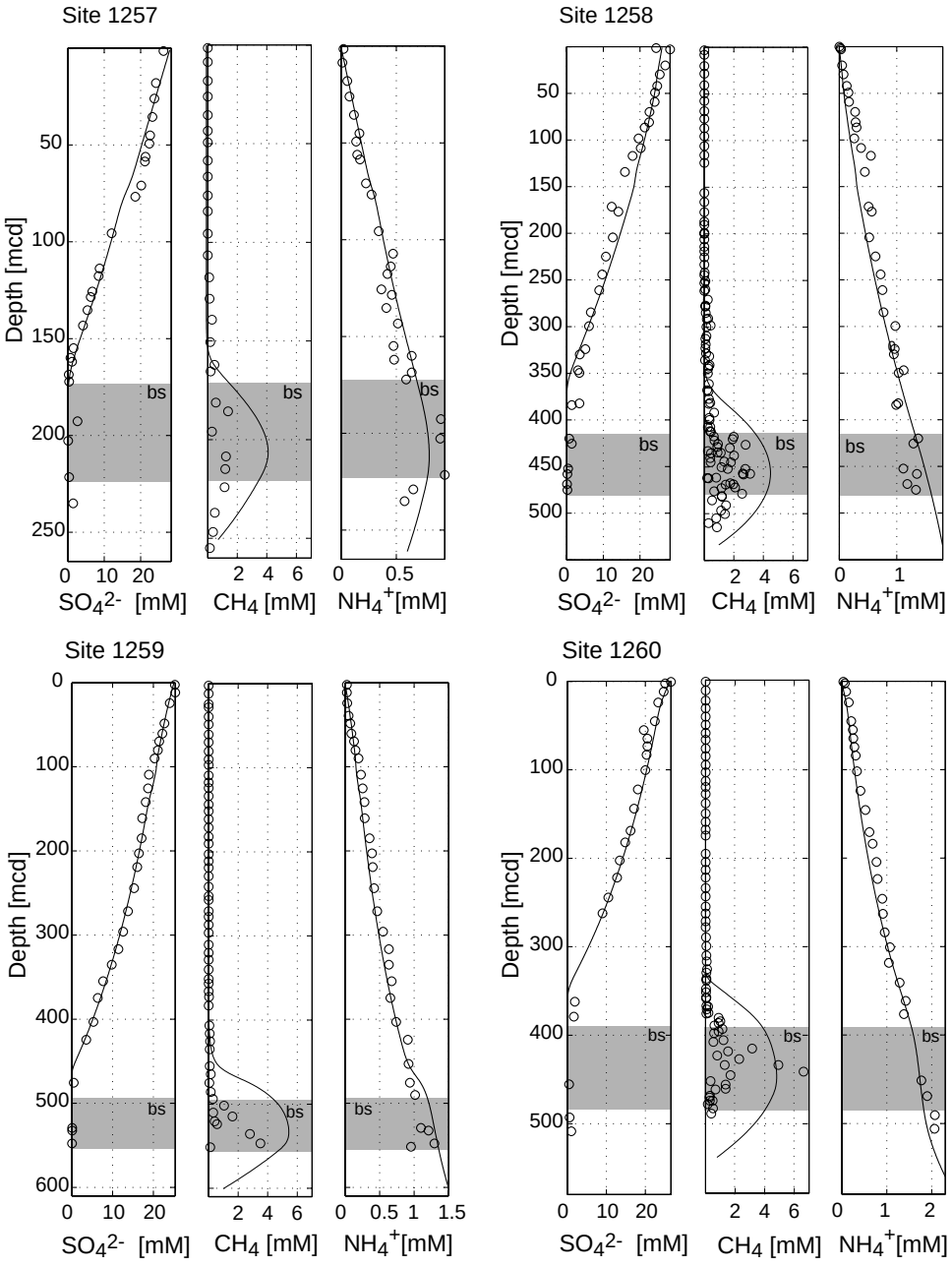


Fig. 8. Simulated and measured concentration profiles of sulfate, methane, and ammonium from sites 1257, 1258, 1259, and 1260. The black shale sequences (bs) are indicated by shaded areas.

observations of black shale sedimentation rates (Shipboard Scientific Party, 2004) allow an estimation of the initial rate constant of organic matter decomposition based on correlations between rate constants and compacted burial velocities. Tromp et al. (1995) evaluated a large data set and proposed the following relationship between burial rate $w$ and anoxic decay constant $k$

$$k = 0.057 \cdot w^{1.94}. \quad (7)$$

Table 5
Degradation rates of organic matter through methanogenesis and depth-integrated degradation rates (rates in μM $a^{-1}$ and μmol $m^{-2}$ $a^{-1}$)

| Site | $R_{G,CH_4}$ | $\int R_{G,CH_4}\,dz$ |
|---|---|---|
| 1257 | 3.27 | 34.74 |
| 1258 | 6.49 | 39.19 |
| 1259 | 9.21–19.10 | 160.86 |
| 1260 | 7.69 | 120.81 |

At Demerara Rise, black shale sediments were deposited with typical rates between $3 \times 10^{-4}$ and $8.4 \times 10^{-4}$ cm $a^{-1}$ (Shipboard Scientific Party, 2004). Assuming Cretaceous conditions and using the averaged organic carbon content of black shales at Demerara Rise ($\bar{C}_{org} = 7.74$ wt.%) (Shipboard Scientific Party, 2004), the

above equations lead to a rate constant of the order of magnitude of $10^{-8}\,a^{-1}$, an extremely high apparent initial age of 38 Ma, and an initial organic carbon content of 12.67 wt.%. This estimate is, however, subjected to a number of uncertainties since the environmental conditions during an OAE can hardly be compared to modern environments. For instance, sea level transgressions during the Cretaceous lead to a reduction of terrigeneous input to the oceans, thus resulting in reduced overall sedimentation rates (Stein et al., 1986). The sedimentation of organic carbon, however, was significantly increased during these times. Moreover, moderate to poor preservation or even absence of microfossils limits biostratigraphic age estimates (Shipboard Scientific Party, 2004) and strong compaction might falsify observations. One can also approach the problem by constraining the initial organic matter contents of Cretaceous sediments to a reasonable range. Using Eq. (6) the apparent initial age can, then, be calculated and plugged into Eq. (5) to determine the temporal evolution of organic matter reactivities. Fig. 9 displays potential, temporal evolutions of organic carbon contents and organic matter reactivities over a period of $10^8$ a and for different initial ages. Anoxic environments and upwelling areas usually reveal organic carbon contents between 2 and 40 wt.% (Stein, 1990). Reasonable values of initial organic carbon contents in the black shales are only obtained when applying relatively high values for the apparent initial age, i.e., low initial decay constants. Thus, an initial organic carbon content of 49 wt.% is determined by assuming an apparent initial age of 0.5 Ma, a value which is even one order of magnitude higher than the value reported for the Central Pacific (Middelburg, 1989), a deep and relative unproductive area with low sediment accumulation rates. This implies that organic matter decomposition at Demerara Rise was characterized by relatively low organic matter reactivities, not exceeding a value of $k = 1 \times 10^{-6}\,a^{-1}$. A possible explanation for these low reactivities might be based on the anoxic conditions, a diagenetic addition of sulfur to organic compounds, as well as elevated C/N values of organic matter that mimic those of land-derived organic matter. Elevated C/N values might be the result of partial alteration of marine organic matter due to a preferential degradation of nitrogen-rich components during sinking to the seafloor (Shipboard Scientific Party, 2004). An incorporation of sulfide into functionalized lipids, favored by high sulfide and low reactive iron concentrations in the black shales, would have led to a stabilization of the organic matter towards further degradation (Sinninghe Damsté et al., 1989; Canfield et al., 1998; Amrani and Aizenshtat, 2004).

As indicated above, organic matter quality may still influence its decomposition in the deep-seated black shales. As a first approximation we assumed that the quality of organic matter in the black shales was homogenized in the course of time and that, degradation of organic matter is exclusively controlled by its content. A correspondence between higher TOC and larger methane gas concentrations confirms this assumption (Shipboard Scientific Party, 2004). Model results, however, indicate the importance of organic matter quality in respect to degradation processes. Model C/N ratios of 20 fall in the lower range of observed values between 16.2 and 44.7, with high average values of around 30. This indicates preferential degradation of better degradable organic matter. Moreover, a slight underestimation of model-calculated, normalized methane concentrations at sites 1259 and 1260 in combination with slightly higher rate constants of methanogenesis points to ongoing organic matter quality dynamics. Excursions from a simple linear relation between sediment organic matter and methane headspace measurements, especially at Sites 1259 and 1260 (Fig. 8), support this assumption

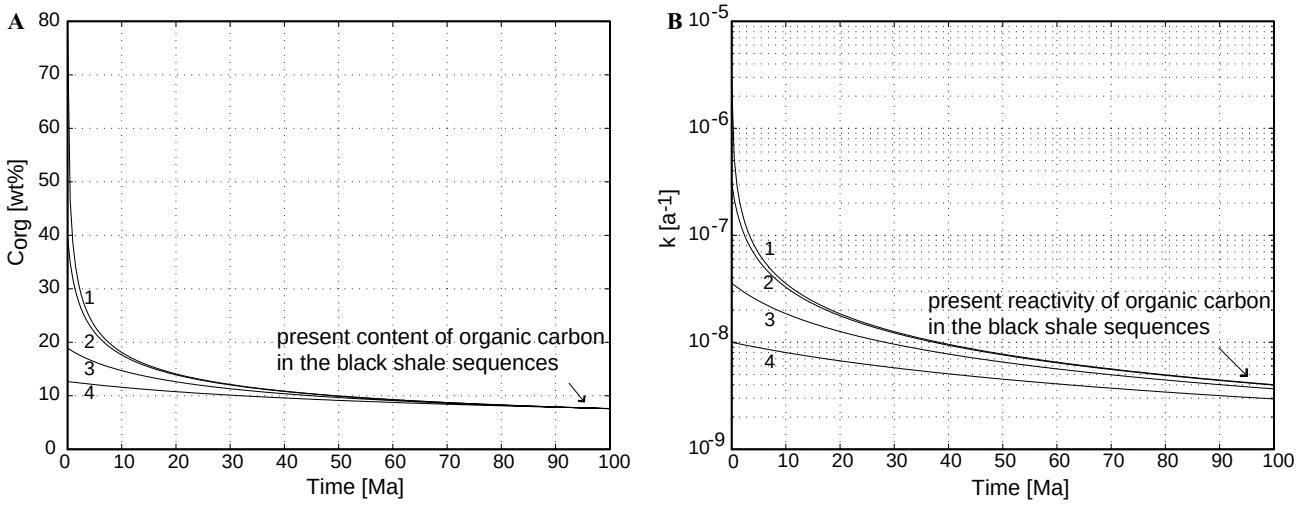


Fig. 9. Temporal evolution of organic carbon (A) content and (B) reactivity for variable apparent initial ages *a*. Organic carbon content and first-order decay parameters have been calculated using the power model of Middelburg (1989) and applying a present organic carbon content of 7.47 wt.% as well as different initial ages (1 = 0.1 Ma, 2 = 1 Ma, 3 = 10 Ma, and 4 = 38.31 Ma).

(Shipboard Scientific Party, 2004). By including a higher number of organic matter fractions, better data fits could be achieved. However, available information is not sufficient to constrain neither the number of fractions nor the distribution of the amount and the quality of organic matter among those fractions. A large number of different possible formulations led to identical results. Therefore, the Multi-G-Model approach is little suitable for the description of organic matter dynamics in sediments from Demerara Rise, since the parameter choice would be purely arbitrary. Although it would potentially provide a better data fit, this formulation would not lead to a better understanding of the system's dynamics. These results indicate the need for a formulation of degradation process in the Deep Biosphere that fully resolves the dynamics on larger time scales.

### 4.4. Anaerobic methane oxidation

Anaerobic methane oxidation (AMO) is a common sink for upward diffusing methane, as well as downward diffusing sulfate in deep marine sediments. This process may account for the consumption of a considerable fraction of the diffusive sulfate flux, thus reducing the availability of sulfate at depth. Reeburgh (1982) estimated that ca. 50% of the diffusive sulfate flux is consumed due to AMO in Cariaco Trench sediments. Niewöhner et al. (1998) and Adler et al. (2000) calculated complete consumption of downward diffusing sulfate during AMO in sediments from the upwelling area off Namibia and the Amazon Fan, respectively. Generally one can assume that depth-integrated methane oxidation rates in the sulfate methane transition zone equal ca. 61–89% of total sulfate reduction (Borowski et al., 2000). At Demerara Rise, upward diffusing methane as well as downward diffusing sulfate are totally consumed in the course of anaerobic methane oxidation above the black shale sequences (Fig. 10). Consequently, sulfate acts as a terminal electron acceptor for the whole ecosystem (D'Hondt et al., 2002).

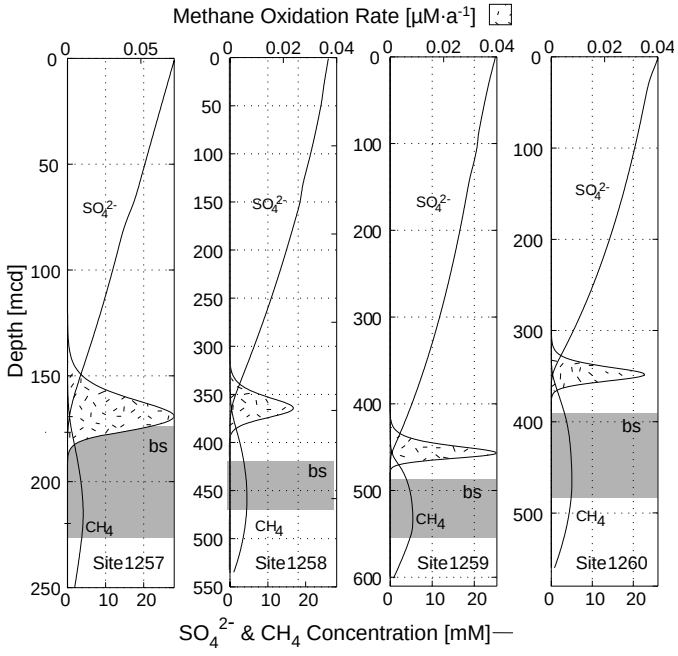


Fig. 10. Simulated sulfate and methane concentration profiles (lines) with anaerobic methane oxidation rates (dotted) in sediments from four drilling sites at Demerara Rise. The black shale sequences (bs) are indicated by shaded areas.

The depth of the sulfate methane transition zone, as well as the availability of sulfate at depth, is exclusively controlled by the production of methane in the black shale sequences. Similar to methanogenic rate constants, model-determined rate constants for AMO (Table 4) are fairly low. These findings reflect the low metabolic activity, which is characteristic for the Deep Biosphere where mean generation times of bacteria are extremely high (Parkes et al., 2000). Geochemical evidence from ODP cores indicates that AMO proceeds very slowly with activities depending on the $CH_4$ flux (Borowski et al., 1999). Simulated methanotrophic sulfate reduction rates reveal peak values of around $10^{-2}$ µM $a^{-1}$ (Fig. 10). Thus, they are significantly lower than the average AMO rates, observed in or modeled for sediments at continental margins and methane seeps (Hinrichs and Boetius, 2002). Nevertheless, recently measured methanotrophic sulfate reduction rates in sediments from ODP Leg 201 (Peru Margin, Deep Biosphere) reveal similar low values between 10 and $4 \times 10^{-1}$ µM $a^{-1}$ in a depth range between 8 and 290 mbsf (Ferdelman T., Kallmeyer J., pers. commun.). It is not surprising that AMO rates in sediments at Demerara Rise fall in the lower range of these values, since the sulfate/methane interface is located deeper in the sediments and concentration gradients are even smaller than those in sediments from ODP Leg 201.

### 4.5. Authigenic barite

Barite may serve as a paleoproductivity proxy (Dymond et al., 1992) and can potentially record neodymium as well as strontium isotopic composition of seawater (Paytan et al., 1993, 1996). However, its use as a geochemical tool is considered to be restricted because of its diagenetic behavior which can alter its sedimentary distribution to a significant extent. An often-observed phenomenon in sediments characterized by high organic matter contents where ongoing sulfate reduction leads to a complete depletion of pore water sulfate at a certain depth is the remobilization of labile, biogenic barites and its subsequent reprecipitation with sulfate from the isotopically heavy residual pool as authigenic concretions or fronts (Brumsack, 1986; van Os et al., 1991; Torres et al., 1996). Increased productivity of surface waters, in combination with increased preservation of organic matter in an anoxic environment are thought to be decisive factors for black shale deposition in the Cretaceous (Erbacher et al., 2001; Wilson and Norris, 2001). Due to the link between biogenic barite formation and suspended organic matter (Dehairs et al., 1980; Bishop, 1988),

sediments at Demerara Rise are characterized by a deep-seated, distinct sediment layer enriched in organic matter and biogenic barite. Additionally, rather low sedimentation rates of sediments younger than middle Eocene in age and a sharp geochemical boundary between the black shales and overlaying sediments provide all the conditions necessary for a formation of an authigenic barite front. According to model results, barite dissolves in the black shales with dissolution rates of about 0.02–0.15 μmol $cm^{-3}$ $a^{-1}$ (Fig. 11) as a consequence of the undersaturation of pore waters with respect to barite. The small amounts of sulfate produced are directly consumed by bacterial processes and

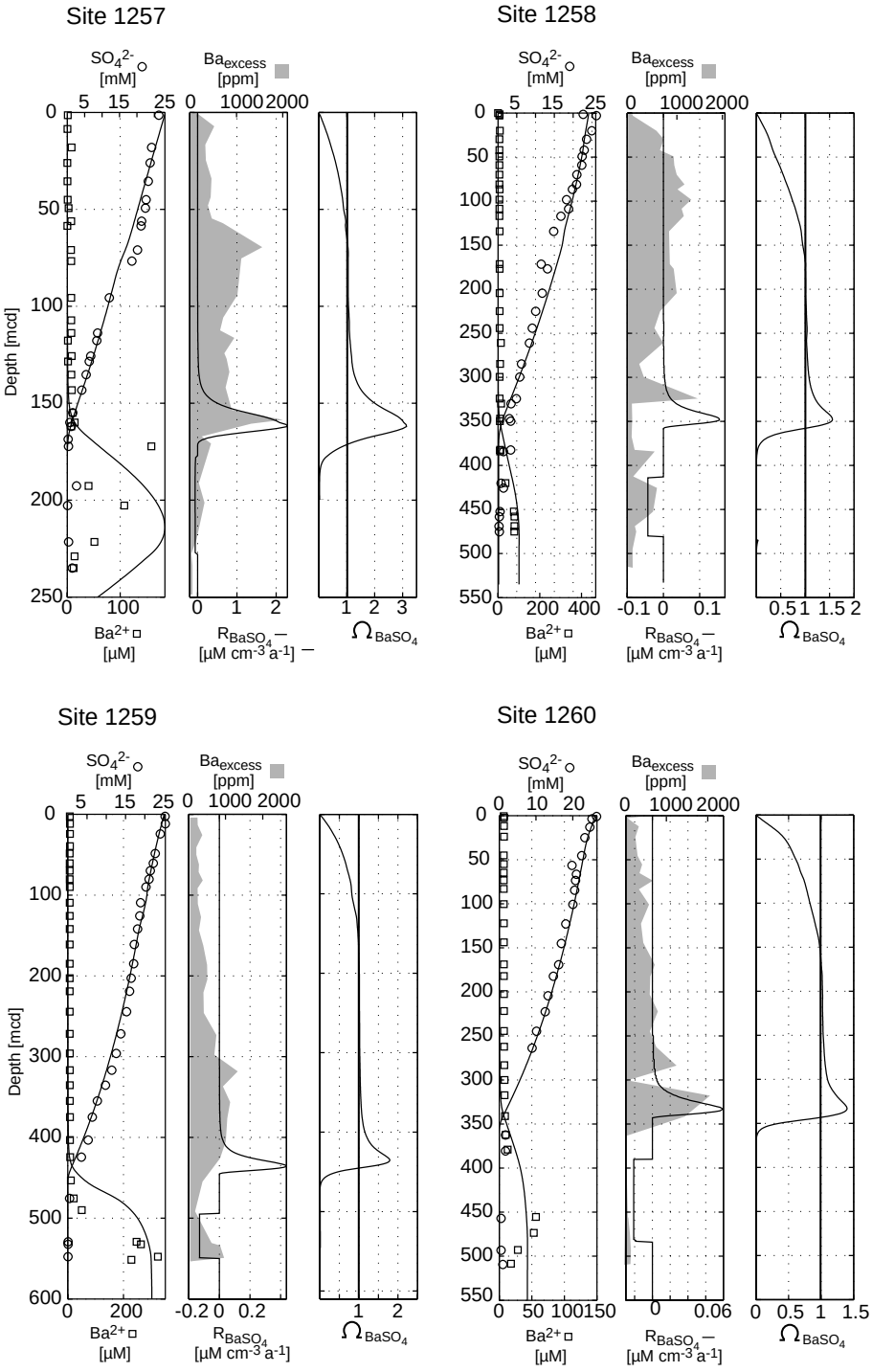


Fig. 11. Barium and sulfate pore water profiles, barite dissolution (negative values)/precipitation (positive values) rates $R_{BaSO_4}$, barium excess values $Ba_{excess}$, and saturation state of interstitial water $\Omega_{BaSO_4}$ with respect to barite at four drilling sites (sites 1257–1260) at Demerara Rise. The solid line in the saturation state plot indicates a saturation of pore waters with respect to barite. Values <1 and values >1 indicate an undersaturation and oversaturation of interstitial waters, respectively. Barium excess values have been calculated by assuming a Ba/Al ratio of 0.00185.

remobilized barium accumulates in the interstitial waters. Dissolved barium concentrations sharply decrease above the black shales, where the available sulfate increases the saturation state of the interstitial waters, leading to the reprecipitation of authigenic barites with rates around 0.06–2.4 μmol $cm^{-3}$ $a^{-1}$ (Fig. 11). While the constrained value for the kinetic constant of barite precipitation is comparable to the rate constant used by Aloisi et al. (2004) in their study of giant cold seeps in the Derugin Basin, the rate constant for barite dissolution used in this model differs from their value. Precipitation of barite in seawater may lead to the incorporation of other minor elements, mostly strontium (Dehairs et al., 1980). The substitution of this strontium into the lattice increases the activity of barite and thus its solubility (McManus et al., 1998). Moreover, barite preservation may be reduced even under suboxic diagenetic conditions in marine sediments for unknown reasons, yet (McManus et al., 1998). These factors are not explicitly formulated in the model and are thus introduced implicitly through the rate constant of barite precipitation, leading to deviations between constrained values in different modeling studies.

Although observed sedimentation rates in younger sediments are low and model results indicate the reprecipitation of barite in a relatively pronounced zone near the sulfate/methane interface, core observations as well as a limited data set of solid phase barium excess values do not reveal the presence of an authigenic front (Fig. 11). In fact, a high number of authigenic barite concretions have been recovered over the whole length of Campanian to Paleogene sediment sequences. The formation of an authigenic front requires the existence of (quasi)steady state conditions over a rather extended period of time. Hence, its absence might indicate the variability of sedimentary states. Model results reveal the strong control of methanogenesis on barite dynamics through the availability of pore water sulfate, thereby pointing to varying intensities of methane production as a cause for nonsteady state conditions in sediments from Demerara Rise. The temporal dynamics of organic matter degradation, characterized by a decrease of the rate constant over eight orders of magnitude (see previous section, and Middelburg, 1989; Bosatta and Agren, 1995), reinforces this hypothesis. Fig. 12 illustrates the effect of an increased and decreased methane flux, caused by an increase or a decrease of the rate constant of methanogenesis, respectively, on the location of the barite precipitation zone. As a consequence of a doubled rate constant of methanogenesis, an enhanced production of methane in the black shales leads to an enhanced diffusional flux out of this lithological unit. Above the black shales, the penetration depth of sulfate is reduced due to an increased consumption of downward diffusing sulfate in the course of AMO. The reduced availability of sulfate in the Campanian chalks results in an upward shift of the barite precipitation zone of about 80 mcd. A decrease of the methanogenic rate constant, however, allows a deeper penetration of sulfate due to a reduced diffusion of methane

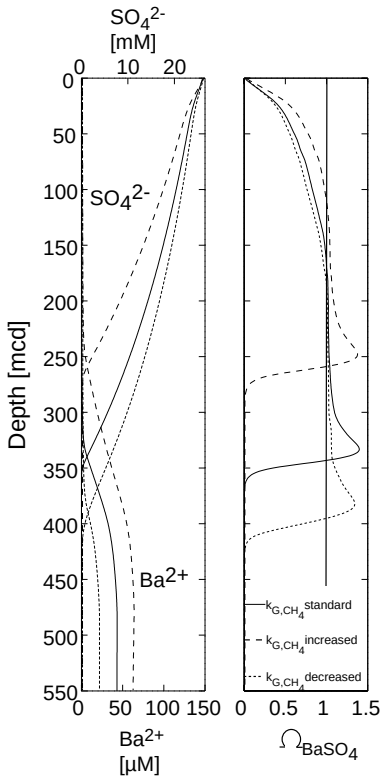


Fig. 12. Variation of the rate constant of methanogenesis $k_{G,CH_4}$ and its influence on barite dynamics. Significant changes in the shape of sulfate, barium, and saturation state depth profiles arise as a consequence of an increase (dashed line) or a decrease bisection (dotted line) of the rate constant by a factor of two.

out of the black shale sequences. The deeper penetration depth of sulfate promotes reprecipitation of barite in greater sediment depths and thus a downward shift of its reprecipitation zone of about 50 mcd. Thus, it can be concluded that the formation of authigenic barite fronts in these sediments was inhibited or already formed fronts have been dissolved as a consequence of the dynamics of methanogenesis. This shows that the distribution of barite in the sediment potentially may serve as a fingerprint for the temporal evolution of biogeochemical processes and that the proxy use of barite is not restricted to sediments lacking strong diagenetic influences if experimental data and model results are carefully combined.

## 5. Conclusion

Interstitial water chemistry at Demerara Rise is mainly influenced by diagenetic processes driven by deep-seated, Santonian, Turonian, and Cenomanian organic matter-rich black shale sequences. Almost 100 Ma after their deposition, these sediments still provide a suitable substrate for ongoing microbial activity in the Deep Biosphere. According to the calibrated model, methanogenesis is the predominant biogeochemical process since it controls the degradation of organic matter as well as the availability of sulfate at depth. Upward diffusing methane as well as

downward diffusing sulfate are totally consumed in the course of AMO above the black shales, driving an enhanced diffusional flux of sulfate from the sediment/water interface to the top of the sulfate depletion zone. Major deviations of sulfate depth profiles from a linear gradient coincide with local porosity maxima or minima. Due to the depth-dependent porosity, two pseudo-advective terms arise in the transport equation, leading to kinked profiles as a consequence of an accelerated or decelerated transport. Hence, other sulfate consuming/producing processes are of minor importance in sediments younger than middle Eocene in age. A complete depletion of sulfate within the black shale sequence promotes the remobilization of biogenic barium. Barite is reprecipitated as authigenic crystals in the zone of increasing sulfate concentrations where pore waters become oversaturated. Model results indicate that temporal dynamics of the degradation processes caused various shifts in the barite precipitation zone during burial, thus inhibiting the formation of an authigenic barite front.

All reaction rates determined by our model are by far lower than those found in shallower sediments due to the low metabolic activities in the Deep Biosphere. The first estimates of rate constants in those depths contribute to a better understanding of this environment. Uncertainties may arise, in particular, due to the poorly constrained lower boundary condition of methane in combination with the dominant influence of methanogenesis in those sediments. Nevertheless, these uncertainties are reduced by a number of additional information provided by the detailed ODP data set from Leg 207. In addition, a comparison with experimentally determined methanotrophic sulfate reduction rates from ODP Leg 201 (Ferdelman T., Kallmeyer J. pers. commun.), other model studies (Aloisi et al., 2004) as well as an empirical $k$–$t$ relationship (Middelburg, 1989) confirms the order of magnitude of model-determined rate constants. Moreover, model results as well as observations indicate that organic matter quality still influences methanogenic processes in the Cretaceous black shales. These findings are challenging our understanding of diagenetic processes and emphasize the need for a formulation of degradation process in the Deep Biosphere that fully resolves the dynamics on larger time scales.

## Acknowledgments

We thank the crew and the scientific party of ODP Leg 207 for their kind support. We are very grateful to Andy Dale and Bernhard Schnetger for their critical comments on earlier drafts of the manuscript and many valuable discussions. Almut Hetzel kindly provided barium data for the squeeze cake samples. A special thanks goes to Tim Ferdelman for a critical discussion of AMO in sediments at Demerara Rise and especially for providing information on sulfate reduction rates in sediments from ODP Leg 201. We are grateful for the valuable comments of Klaus Wallmann and one anonymous reviewer. This research was supported by the German Science Foundation (ODP-SPP, Br 775/16, and Br 775/17).

*Associate editor:* Jack J. Middelburg

## Appendix A

### A.1. Transport

A large number of different processes, such as advection, diffusion, porosity or temperature gradients, may control the shape of observed concentration profiles. Thus, the choice of processes during model design will have a direct effect on the estimates of chemical kinetic parameters. Yet, one always aims for the simplest model that is potentially able to explain the observed distributions. Processes, which have a negligible effect on concentration profiles, should, therefore, be excluded.

The Peclet number $Pe = \frac{v \cdot L}{D}$ indicates the relative importance of advective to diffusive transport over a chosen length scale $L$. As in most deep sea sediments, present sedimentation rates at Demerara Rise are, generally, small ($6.7 \times 10^{-6}$–$15 \times 10^{-6}\,\mathrm{m\,a^{-1}}$) (Shipboard Scientific Party, 2004) and transport processes are, thus, diffusion dominated. Even if one considers the transport of dissolved species over the length of the whole sediment column, Peclet numbers still reveal values smaller than 1 (Table A1). In sediments at Demerara Rise, most of the biogeochemical transformations act over depth scales of about 100 m and advection related to the deposition of sediment is, therefore, negligible. Variations by some small factor, which may arise as a consequence of neglecting advection, may be admissible, if they are viewed within the scope of other uncertainties, such as measurement errors or diffusion coefficients.

For a dissolved species undergoing transport by molecular diffusion, the temporal change in concentration due to transport processes can be formulated as

$$\frac{\partial C_i}{\partial t}\Big|_{\text{transport}} = D_i' \frac{\partial C_i^2}{\partial z^2} + \left(\frac{D_i'}{\phi}\frac{\partial \phi}{\partial z} + \frac{\partial D_i'}{\partial z}\right)\frac{\partial C_i}{\partial z}, \qquad \text{(A.1)}$$

where $\phi$ is the porosity. The effective diffusion coefficients $D_i'$ for dissolved species are determined by correcting the

Table A1
Peclet number $Pe = \frac{v \cdot L}{D}$ for the transport of barium ($D_{\mathrm{Ba}} = 0.012\,\mathrm{m^2\,a^{-1}}$) over the length scales $L$ in meter

| Site | $L$ | 50 | 150 | 200 | $L_{\max}$ |
|---|---|---|---|---|---|
| 1257 | *Pe* | 0.04 | 0.11 | 0.15 | 0.17 |
| 1258 | *Pe* | 0.06 | 0.19 | 0.25 | 0.59 |
| 1259 | *Pe* | 0.05 | 0.16 | 0.22 | 0.59 |
| 1260 | *Pe* | 0.03 | 0.08 | 0.11 | 0.27 |

The maximum length scales equal the lower limit of the black shale sequences at each site ($L_{\max,1257} = 227$ m, $L_{\max,1258} = 475$ m, $L_{\max,1259} = 549$ m, and $L_{\max,1260} = 484$ m). Advection velocities were chosen according to current sedimentation rates of the uppermost sediment units (Shipboard Scientific Party, 2004).

diffusion coefficients in free solution $D_{0,i}$ (Boudreau, 1997) for tortuosity $\Theta^2$

$$D_i' = \frac{D_{0,i}}{\Theta^2}, \tag{A.2}$$

where the tortuosity $\Theta^2$ is calculated by means of porosity according to a relationship proposed by Boudreau (1997),

$$\Theta^2 = 1 - 2 \cdot \ln \phi. \tag{A.3}$$

It is important to note that two pseudo-advective terms arise in the conservation equation as a consequence of diffusion through a porosity gradient.

### A.2. Biogeochemical processes

The degradation of organic matter is the driving force behind the biogeochemical reaction network in sediments. It is formulated according to the G-Model (Berner, 1980). Since the remineralization of organic matter in subsurface (>1.5 m) sediments is mainly controlled by sulfate reduction and methanogenesis (Jørgensen, 1982; D'Hondt et al., 2002), the G-Model approach simply reads,

$$R_G = -f_{ox} k_G [CH_2O]. \tag{A.4}$$

The overall rate of carbon degradation $R_G$ is proportional to the total concentration of organic matter $[CH_2O]$. A term $f_{ox}$ accounts for the oxidant limitation which equals 1 ($f_{CH_4} = 1$) for methanogenesis where no external oxidant is involved. The dependence of the rate of organic matter oxidation on sulfate availability is described by the Monod law

$$f_{SO_4} = \frac{[SO_4^{2-}]}{[SO_4^{2-}] + K_S}, \tag{A.5}$$

where the half-saturation constant for sulfate utilization $K_S$ is 1.6 mM (Boudreau and Westrich, 1984).

Sulfate concentration greater then 1–2 mM exert no significant influence on AMO rates. We therefore use a Monod dependence on the sulfate concentration with a Monod constant $K_{S,AMO}$ of 1 mM (Nauhaus et al., 1995). Rate laws of a similar type have already been used successfully by other authors (e.g., Treude et al., 2003), even though the mechanism of AMO is poorly understood

$$R_{AMO} = k_{AMO} \cdot [CH_4] \frac{[SO_4^{2-}]}{K_{S,AMO} + [SO_4^{2-}]}. \tag{A.6}$$

The total depletion of sulfate in the sulfate reduction zone can promote the dissolution of biogenic barite in sediments due to a shift in equilibrium. The relatively fast rate of mineral dissolution and precipitation allows a solely thermodynamic formulation. Reaction rates of dissolution and precipitation are expressed in the form of empirical rate laws following experimental results (Christy and Putnis, 1993; Bosbach, 2002):

$$R_{BaSO_4,diss} = k_{BaSO_4,diss} [BaSO_4](\Omega - 1), \tag{A.7}$$

for $\Omega < 1$ and

$$R_{BaSO_4,prec} = k_{BaSO_4,prec} (1 - \Omega)^2, \tag{A.8}$$

for $\Omega > 1$,where $k_{BaSO_4,diss}$ and $k_{BaSO_4,prec}$ are the rate constants for dissolution and precipitation, respectively. The state of saturation of the pore water solution $\Omega$ is defined by the ratio of the ion activity product over the corresponding stoichiometric solubility product equilibrium constant $K_{sp}$,

$$\Omega = \frac{[SO_4^{2-}][Ba^{2+}]}{K_{sp}}. \tag{A.9}$$

Values of $K_{sp}$ are calculated as a function of salinity $S$ and temperature $T$ (kelvin) using an empirical relation provided by Rushdi et al. (2000)

$$\ln K_{sp} = A + B \cdot \ln T + \frac{C}{T} + D \cdot S^n, \tag{A.10}$$

where the constants $A$, $B$, $C$, $D$, and $n$ are 247.6157, −38.3226, −15421.20, 1.2645, and 0.3, respectively. In addition to temperature, the effect of pressure on $K_{sp}$ can play an important role in deep sediment depths with an increasing weight of the overlaying sediment and the water column. Therefore, the stoichiometric solubility product equilibrium constant at a pressure of 0 atmospheres, $K_{sp}^0$, is corrected for the effect of pressure using an equation of the form (Rushdi et al., 2000)

$$\ln \frac{K_{sp}^p}{K_{sp}^0} = (\upsilon_0 + \upsilon_1 T_C) \cdot \frac{P}{RT_K} + \frac{1}{2}(k_0 + k_1 T_C) \cdot \frac{P^2}{RT_K}, \tag{A.11}$$

where the constants are $\upsilon_0 = 45.61714\ cm^3\ mol^{-1}$, $\upsilon_1 = -0.25097\ cm^3\ mol^{-1}$, $k_0 = -14.445 \times 10^{-3}\ cm^3\ mol^{-1}\ atm^{-1}$, and $k_1 = 1.251 \times 10^{-4}\ cm^3\ mol^{-1}\ atm^{-1}$. The temperatures $T_C$ and $T_K$ are given in C and kelvin, respectively. $R$ is the gas constant in $J\ mol^{-1}\ K^{-1}$ and $P$ the pressure in atmosphere.

Ammonium is a typical product of organic matter degradation, reveals maximum concentrations in the zone of organic matter decomposition, and diffuses upwards in the sediment column. Adsorption is a fairly fast process with respect to most microbial controlled processes and can therefore be assumed to be in steady state, i.e., adsorbed ammonium equals dissolved ammonium times an equilibrium constant $K_{NH_4} = 1.3$ (Berner, 1980). Consequently, adsorption slows down ammonium dynamics (Berner, 1980).

## References

Adler, M., Hensen, C., Kasten, S., Schulz, H.D., 2000. Computer simulation of deep sulfate reduction in sediments of the Amazon Fan. *International Journal of Earth Sciences* **88**, 641–654.

Aloisi, G., Wallmann, K., Bollwerk, S., Derkachev, A., 2004. The effect of dissolved barium on biogeochemical processes at cold seeps. *Geochimica et Cosmochimica Acta* **68**, 1735–1748.

Amrani, A., Aizenshtat, Z., 2004. Reaction of polysulfide anions with α, β unsaturated isoprenoid aldehydes in aquatic media: simulation of oceanic conditions. *Organic Geochemistry* **35**, 909–921.

Arthur, M., Brumsack, H.-J., Jenkyns, H., Schlanger, S., 1990. Stratigraphy, geochemistry, and palaeoceanography of organic carbon-rich Cretaceous sequences. In: *Cretaceous Resources, Events and Rhythms*. Kluwer, Dordrecht, pp. 75–119.

Berner, R.A., 1980. *Early Diagenesis: A Theoretical Approach*. Princeton University Press, Princeton, NJ.

Bishop, J., 1988. The barite–opal–organic carbon association in oceanic particulate matter. *Nature* **332**, 341–343.

Borowski, W., Hoehler, T., Alperin, M., Rodriguez, N., Paull, C., 2000. Significance of anaerobic methane oxidation in methane-rich sediments overlying the Blake Ridge gas hydrates. *Proceedings of ODP Scientific Results* **164**, 87–99.

Borowski, W., Paull, C., Ussler, W., 1999. Global and local variations of interstitial sulfate gradients in deep-water, continental margin sediments: sensitivity to underlying methane and gas hydrates. *Marine Geology* **159**, 131–154.

Bosatta, E., Agren, G., 1995. The power and reactive continuum models as particular cases of the q-theory of organic matter dynamics. *Geochimica et Cosmochimica Acta* **59**, 3833–3835.

Bosbach, D., 2002. Linking molecular-scale barite precipitation mechanisms with macroscopic crystal growth rates. Geochemical Society, Houston. Special Publications **7**, 97–110.

Boudreau, B.P., 1997. *Diagenetic Models and their Implementation: Modelling Transport and Reactions in Aquatic Sediments*. Springer, Berlin, Heidelberg, New York.

Boudreau, B.P., Westrich, J.T., 1984. The dependence of bacterial sulfate reduction on sulfate concentration in marine sediments. *Geochimica et Cosmochimica Acta* **48**, 2503–2516.

Bréhéret, G., Brumsack, H.-J., 2000. Barite concretions as evidence of pauses in sedimentation in the Marnes Bleues formation of the Vocontian Basin (SE France). *Sedimentary Geology* **130**, 205–228.

Brumsack, H.-J., 1986. The inorganic geochemistry of Cretaceous black shales (DSDP Leg 41) in comparison to modern upwelling sediments from the Gulf of California. In: *North Atlantic Palaeoceanography*. Blackwell, London, pp. 447–462.

Brumsack, H.-J., 2005. The trace metal content of recent organic carbon-rich sediments: implications for Cretaceous black shale formation. *Palaeogeography, Palaeoclimatology, Palaeoecology* (in press).

Brumsack, H.J., Gieskes, J., 1983. Interstitial water trace metal chemistry of laminated sediments from the Gulf of California Mexico. *Marine Chemistry* **14**, 86–106.

Canfield, D., Boudreau, B., Mucci, A., Gundersen, J., 1998. The early diagenetic formation of organic sulfur in the sediments of Mangrove Lake, Bermuda. *Geochimica et Cosmochimica Acta* **62**, 767–781.

Canfield, D.E., 1994. Factors influencing organic carbon preservation in marine sediments. *Chemical Geology* **114**, 315–329.

Christy, A.G., Putnis, A., 1993. The kinetics of barite dissolution and precipitation in water and sodium chloride brines at 44–85 C. *Geochimica et Cosmochimica Acta* **57**, 2161–2168.

Church, T., Wohlgemuth, K., 1972. Marine barite saturation. *Earth and Planetary Science Letters* **15**, 35–44.

Coolen, M., Cypionka, H., Sass, A., Sass, H., Overmann, J., 2002. Ongoing modification of mediterranean pleistocene sapropels mediated by prokaryotes. *Science* **296**, 2407–2410.

Cragg, B., Parkes, R., Fry, J., Herbert, R., Wimpenny, J., Getliff, J., 1992. Bacterial biomass and activity profiles within deep sediment layers. In: *Proceedings of the Ocean Drilling Program, Scientific Results*, pp. 607–619.

Dehairs, F., Chesselet, R., Jedwab, J., 1980. Discrete suspended particles of barite and the barium cycle in the open ocean. *Earth and Planetary Science Letters* **49**, 529–550.

D'Hondt, S., Jørgensen, B., Miller, D., Batzke, A., Blake, R., Cragg, B., Cypionka, H., Dickens, G., Ferdelman, T., Hinrichs, K.-U., Holm, N., Mitterer, R., Spivack, A., Wang, G., Bekins, B., Engelen, B., Ford, K., Gettemy, G., Rutherford, S., Sass, H., Skilbeck, C., Aiello, I., Gurin, G., House, C., Inagaki, F., Meister, P., Naehr, T., Niitsuma, S., Parkes, R., Schippers, A., Smith, D., Teske, A., Wiegel, J., Naranjo Padilla, Solis Acosta, J., . Distributions of microbial activities in deep subseafloor sediments. *Science* **306**, 2216–2221.

D'Hondt, S., Jørgensen, B.B., Miller, D.J., ODP Leg 201 Science Party, 2003. Leg 201 summary. In: *Proceedings of the Ocean Drilling Program, Initial Reports*, vol. 201, pp. 1–17.

D'Hondt, S., Rutherford, S., Spivack, A., 2002. Metabolic activity of subsurface life in deep-sea sediments. *Science* **295**, 2067–2069.

Dickins, H., van Vleet, E., 1992. Archaebacterial activity in the Orca Basin determined by the isolation of characteristic isopranyl ether-linked lipids. *Deep Sea Research* **39**, 521–536.

Dymond, J., Suess, E., Lyle, R., 1992. Barium in deep sea sediment: a geochemical proxy for paleoproductivity. *Paleoceanography* **7**, 163–174.

Eder, W., Jahnke, L., Schmidt, M., Huberl, R., 2001. Microbial diversity of the brine–seawater interface of the Kebrit Deep, Red Sea, Studied via 16S rRNA gene sequences and cultivation methods. *Applied and Environmental Microbiology* **67**, 3075–3085.

Erbacher, J., Huber, B., Norris, R., Markey, M., 2001. Intensified thermohaline stratification as a possible cause for an ocean anoxic event in the Cretaceous period. *Nature* **409**, 325–327.

Gieskes, J., Gamo, T., Brumsack, H.-J., 1991. Chemical methods for interstitial waters of marine sediments, based on deep sea drill cores. *JOIDES Resolution*. ODP Technical Note 15.

Hetzel, A., 2003. *Haupt- und Spurenmetallverteilungen in Sedimenten des Demerara Rise (ODP Leg 207)*. Master's thesis, Carl-von-Ossietzky Universität Oldenburg.

Hinrichs, K.-U., Boetius, A., 2002. The anaerobic oxidation of methane: new insights in microbial ecology and biogeochemistry. In: *Ocean Margin Systems*. Springer, Berlin, Heidelberg, pp. 457–477.

Jørgensen, B.B., 1982. Mineralization of organic matter in the sea bed—the role of sulphate reduction. *Nature* **296**, 643–645.

Kotelnikova, S., 1992. Microbial production and oxidation of methane in deep subsurface. *Earth Science Reviews* **58**, 367–395.

Krumholz, L., Harris, S., Suflita, J., 2002. Anaerobic microbial growth from components of Cretaceous shales. *Geomicrobiology* **19**, 593–602.

Krumholz, L., McKinley, J., Ulrich, G., Suflita, J., 1997. Confined subsurface microbial communities in Cretaceous rock. *Nature* **386**, 64–66.

Kvenvolden, K., McDonald, T.J., 1986. Organic geochemistry on the JOIDES resolution—an assay. ODP Technical Notes 6.

Manheim, F., Sayles, F., 1974. Composition and origin of interstitial waters of marine sediments, based on deep sea drill cores*The Sea*, vol. 5. Wiley-Interscience, New York, pp. 527–568.

McManus, W., Berelson, W., Klinkhammer, G., Johnson, K., Coale, K., Anderson, R., Kumar, N., Burdige, D., Hammond, D., Brumsack, H.-J., McCorkle, D., Rushdi, A., 1998. Geochemistry of barium in marine sediments: implications for its use as a paleoproxy. *Geochimica et Cosmochimica Acta* **62**, 3453–3473.

Meyers, P., Forster, A., Sturt, H., Shipboard Scientific Party, 2004. Microbial gases in black shale sequences on the Demerara Rise. In: *Proceedings of the Ocean Drilling Program, Initial Reports 207 [CD-ROM]*, vols. 1–18 [CD-ROM]. (Available from: Ocean Drilling Program, Texas A&M University, College Station, TX 77845-9547, USA).

Middelburg, J.J., 1989. A simple rate model for organic matter decomposition in marine sediments. *Geochimica et Cosmochimica Acta* **53**, 1577–1581.

Murray, R.W., Miller, D., Kryc, K., 2000. Analysis of major and trace elements in rocks, sediments, and interstitial waters by inductively coupled plasma-atomic emission spectrometry (ICP-AES). ODP Technical Note 29.

Nauhaus, K., Boetius, A., Krüger, M., Widdel, F., 1995. In vitro demonstration of anaerobic oxidation of methane coupled to sulphate reduction in sediment from marine gas hydrate area. *Environmental Microbiology* **4**, 298–305.

Niewöhner, C., Hensen, C., Kasten, S., Zabel, M., Schulz, H., 1998. Deep sulfate reduction completely mediated by anaerobic methane oxidation

in sediments of the upwelling area off Namibia. *Geochemica et Cosmochimica Acta* **62**, 455–464.

Oremland, R.S., Polcin, S., 1982. Methanogenesis and sulfate reduction: competitive and noncompetitive substrates in estuarine sediments. *Applied Environmental Microbiology* **44**, 1270–1276.

Oren, A., 2002. Diversity of halophilic microorganisms: environments, phylogeny, physiology and applications. *Journal of Industrial Microbiology and Biotechnology* **28**, 56–63.

Parkes, R., Cragg, B., Wellsbury, P., 2000. Recent studies on bacterial populations and processes in subseafloor sediments: a review. *Hydrogeology* **8**, 11–28.

Paytan, A., Kastner, M., Chavez, F., 1996. Glacial to interglacial fluctuations in productivity in the Equatorial Pacific as indicated by marine barite. *Science* **274**, 1355–1357.

Paytan, A., Kastner, M., Martin, E., Macdougall, J., Herbert, T., 1993. Marine barite as a monitor of seawater strontium isotope composition. *Nature* **366**, 445–449.

Reeburgh, W., 1982. A major sink and flux control for methane in marine sediments: anaerobic consumption. In: Fanning, K.A., Manheim, F.T. (Eds.). The Dynamic Environment of the Ocean Floor, pp. 203–217.

Rushdi, A.I., McManus, J., Collier, R.W., 2000. Marine barite and celestite saturation in seawater. *Marine Chemistry* **69**, 19–31.

Schlanger, S., Jenkyns, H., 1976. Cretaceous oceanic anoxic events: causes and consequences. *Geochimica et Cosmochimica Acta* **55**, 179–184.

Shipboard Scientific Party, 1990. In: *Proceedings of the Ocean Drilling Program, Initial Reports*. College Station, TX (Ocean Drilling Program), pp. 331–334 (Chapter 122).

Shipboard Scientific Party, 1996. In: *Proceedings of the Ocean Drilling Program, Initial Reports*. College Station, TX (Ocean Drilling Program), pp. 65–150 (Chapter 159).

Shipboard Scientific Party, 2004. In: *Proceedings of the Ocean Drilling Program, Initial Reports 207 [CD-ROM]*, vols. 1–89 [CD-ROM]. (Available from: Ocean Drilling Program, Texas A&M University, College Station, TX 77845-9547, USA, Ch. Leg 207 summary).

Sinninghe Damsté, J., Rijpstra, W., Kock-van Dalen, A., de Lewuw, J., Schenck, P., 1989. Quenching of labile functionalised lipids by inorganic sulphur species: evidences for the formation of sedimentary organic sulphur compounds at the early stages of diagenesis. *Geochimica et Cosmochimica Acta* **53**, 1343–1355.

Stein, R., 1990. Organic carbon content/sedimentation rate relationship and its paleoenvironmental significance for marine sediments. *Geo-Marine Letters* **10**, 37–44.

Stein, R., Rullköter, J., Welte, D., 1986. Accumulation of organic-carbon-rich sediments in the Late Jurassic and Cretaceous Atlantic Ocean: a synthesis. *Chemical Geology* **56**, 1–32.

Tarafa, M., Whelan, J., Oremland, R., Smith, R., 1987. Evidence of microbiological activity in Leg 95 (New Jersey Transect) sediments. Initial Reports DSDP,95. U.S. Govt. Printing Office, Washington, pp. 635–640.

Torres, M.E., Brumsack, H.J., Bohrmann, G., Emeis, K.C., 1996. Barite fronts in continental margin sediments: a new look at barium remobilization in the zone of sulfate reduction and formation of heavy barites in diagenetic fronts. *Chemical Geology* **127**, 125–139.

Treude, T., Boetius, A., Knittel, K., Wallmann, K., Jørgensen, B.B., 2003. Anaerobic oxidation of methane above gas hydrates at Hydrate Ridge, NE Pacific Ocean. *Marine Ecology Progress Series* **264**, 1–14.

Tromp, T., Van Cappellen, P., Key, R., 1995. A global model for the early diagenesis of organic carbon and organic phosphorus in marine sediments. *Geochimica et Cosmochimica Acta* **59**, 1259–1284.

van der Wielen, P., Bolhuis, H., Borin, S., Daffonchio, D., Corselli, C., Giuliano, L., de Lange, G., Huebner, A., Varnavas, S., Thomson, J., Tamburini, C., Marty, D., McGenity, T., Timmis, K., Party, B.S., 2005. The enigma of prokaryotic life in deep hypersaline anoxic basins. *Science* **307**, 121–123.

van Os, B., Middelburg, J., de Lange, G., 1991. Possible diagenetic mobilization of barium in sapropelic sediment from eastern Mediterranean. *Marine Geology* **100**, 123–136.

Wehausen, R., Schnetger, B., Brumsack, H.-J., De Lange, G., 1999. Determination of major and minor ions in brines by X-ray fluorescence spectrometry: comparison with other common analytical methods. *X-ray Spectrometry* **28**, 168–172.

Whelan, J., Oremland, R., Tarafa, M., Smith, R., Howarth, R., Lee, C., 1986. Evidence for sulfate-reducing and methane producing microorganisms in sediments from Sites 618, 619, and 622. Initial Reports DSDP,96. U.S. Govt. Printing Office, Washington, pp. 767–775.

Whiteman, W., Coleman, D., Wiebe, W., 1998. Prokaryotes: the unseen majority. *Proceedings of National Academic Sciences of the United States of America* **95**, 6578–6583.

Wilson, P., Norris, R., 2001. Warm tropical ocean surface and and global anoxia during the mid-Cretaceous period. *Nature* **412**, 425–429.